Dispersion of mixtures of submicrometer and nanometer sized titanias to obtain porous bodies

M. Vicent,[1] E. Sánchez,[1] T. Molina,[2] M.I. Nieto,[2] R. Moreno[2]

[1] Instituto de Tecnología Cerámica (ITC), Asociación de Investigación de las Industrias Cerámicas (AICE), Universitat Jaume I (UJI), E-12006 Castellón, Spain.

[2] Instituto de Cerámica y Vidrio (ICV), CSIC, E-28049 Madrid, Spain.

Abstract

The stability and rheological behaviour of bimodal titania suspensions was studied. Bimodal mixtures were prepared by mixing nanosized TiO_2 powders with an average primary size of ~20-40 nm and surface area of ~50 m^2/g and/or a colloidal titania suspension of the same nanopowders dispersed in water with a submicrometer sized titania. The dispersing conditions were studied as a function of pH, type and content of dispersant, and sonication time for a constant solids content of 30 vol.% (62 wt%). The mixtures were slip cast and presintered at low temperatures (800–1000 ºC) in order to obtain porous materials with anatase as the major phase. The pore size distribution, microstructure and phase composition were characterised using MIP, SEM and XRD techniques, respectively.

Keywords: TiO_2, Suspensions, Rheology, Slip casting, Porous ceramics

Introduction

Titania (TiO_2) based materials have a great attractive due to their photocatalytic activity [1]. TiO_2 occurs naturally as minerals with rutile, anatase and brookite phases. The rutile and anatase phases have been widely studied and have significant technological uses related mainly to their optical properties since both are transparent in

the visible range and absorb in the near ultraviolet. Although there is some controversy, it seems that a mixture of anatase/rutile phases is desirable to get enhanced photoactivity [2,3]. Other methods to improve photoactivity include enlargement of surface area, loading of noble metal clusters [4], doping with appropriate elements [5,6], or using special morphologies such as hollow spheres [7,8]. As a photocatalyst, TiO_2 can be used in the form of powder and thin films [9].

There is a growing interest to develop reliable, economic and environmentally-friendly methods for manufacturing thin and thick coatings and layered systems. Layered ceramics and coatings have received increasing attention because of their ability to satisfy critical requisites that are not fulfilled by any monolithic material [10]. Current methods for producing these coatings include chemical and physical vapour deposition (CVD and PVD), thermal spraying, self-propagating high-temperature synthesis (SHS), etc. [11,12]. Regarding thermal spraying, an example is atmospheric plasma spraying (APS) that allows the production of finely nanostructured coatings [13-16].

Most studies concerning the dispersion and stability of TiO_2 suspensions have been carried out using submicrometer and micrometer sized particles [16,17]. However, the use of TiO_2 nanoparticles is continuously increasing. Handling of nanoparticulate systems is difficult and hazardous due to their volatility and the subsequent inhalation risks. One of the most extended routes to allow handling of nanoparticulate systems is the production of free-flowing agglomerates from colloidal suspensions subjected to a controlled drying process, such as spray and freeze drying [18-23].

For the production of nanostructured granules the dispersion and manipulation of the nanoparticles is a key step. The characteristics of the suspension determine the morphology of the granules and then, the properties of the final ceramic product. Many

studies have reported the dispersion and stability of suspensions of nanosized ceramic powders, focusing on the effect of deflocculant concentration and pH on the rheological properties of differently prepared suspensions. For nanosized titania, Fazio et al. [24] reported the dispersion and stabilisation of two commercial nanopowders which were an anatase and a rutile titania. Large zeta potentials were obtained for these commercial nanopowders dispersed with a polyelectrolyte. Faure et al. [25] optimised the stability of an anatase-rutile nanotitania suspension in terms of dispersing agents concentration and pH by measuring the rheological properties of differently prepared suspensions. In this case, 25 wt% solids content nanosuspensions were used for spray-drying. Vicent et al. studied the dispersion of titania nanopowders in water and established a simple route to prepare concentrated suspensions of nanoparticles by dispersing the nanopowders using commercially available colloidal suspensions as a dispersing medium [26,27]. This allowed to increase the solids loading to $\geq$ 30 vol.% (i.e. > 65 wt%) while maintaining a good flowability.

The dispersion of heterogeneous mixtures is complex due to the very different colloidal behaviour of each phase. Some authors have demonstrated that it was possible to enhance sintering through green state deformation processing, as stated for alumina submicrometer sized particles [28,29]. When homogeneous dispersions of two phases with very different size or shape are needed, heterocoagulation can be a suitable route to force the uniformity through strong electrostatic interactions. This has been demonstrated to be very effective for the manufacture of carbon nanotubes reinforced ceramics or the production of mullite by reaction sintering by a core-shell reaction [30,31].

Considering the difficulties associated to the densification of nanostructured materials, the manufacture of porous titania based photocatalysts with high surface area

is receiving increased attention for water treatment applications [32,33]. Porous materials can be produced with a number of techniques, such as the use of sacrificial templates, replication methods, freeze drying and direct foaming using surfactants and polymerizable monomers [34,35].

The aim of this work is to study the colloidal stability and rheological behaviour of mixtures of submicrometer and nanometer sized titania and to evaluate the feasibility to produce porous bodies at low temperature by a simple colloidal filtration route.

Experimental

As starting materials two powders with different particle size and a colloidal suspension of TiO_2 were used in this study: a submicron sized anatase-TiO_2 (808, Merck, Germany), and a nanosized powder (Aeroxide® P25, Degussa-Evonik, Germany) that contains anatase and rutile phases in a ratio of about 4:1 [36]. A commercial colloidal suspension (AERODISP® W740X, Degussa-Evonik, Germany), was also used. The main characteristics of the starting powders are summarised in table 1.

The particle size distributions were determined by laser diffraction (Mastersizer S, Malvern, Worcestershire, United Kingdom), and dynamic light scattering (Nanosizer NanoZS, Malvern, United Kingdom), for submicrometer and nanometer sized powders, respectively. The specific surface area was measured by the N_2 adsorption method (Monosorb Surface Area Analyser MS13, Quantachrome Co., USA). A complete characterisation of the P-25 nanopowder was done in a previous work [26]. Differential thermal analysis and thermogravimetric analyses (DTA/TG, STAY09, Netzsch, Germany) showed that the P25-powder had a weight loss lower than 2.5 wt%, while the dry powder obtained from the W740X-suspension had a weight loss of 4.5 wt%. This

evidences the presence of some organics at the surface which can difficult the adsorption of deflocculants [27].

The colloidal behaviour of the powders and the colloidal suspension was studied through zeta potential measurements as a function of deflocculant content and pH using a Zetasizer NanoZS instrument (Malvern, United Kingdom), based in the laser Doppler velocimetry technique. The best accuracy of zeta potential measurements was reached for suspensions diluted to a concentration of titania of 0.005 wt%, using KCl 0.01M as inert electrolyte. pH values were determined with a pH-meter (716 DMS Titrine, Metrohm, Switzerland) and were adjusted with HCl and KOH solutions (0.1 and 0.01M). To improve the dispersion state, an ultrasounds probe (UP 400S, Dr Hielscher GmbH, Germany) was used for a sonication time of 30 seconds.

In a previous work, the colloidal behaviour of the dry P25 nanopowder and the colloidal W740X suspension was reported [27]. According to that study, a commercial salt of polyacrylic acid-based polyelectrolite (DURAMAX^{TM} D-3005, Dow Chemicals, USA), with 35 wt% active matter, was used. This deflocculant was used also for the bimodal mixtures studied in the present work.

Concentrated suspensions with a total solids contents of 30 vol.% were prepared mixing 50 wt% of nanometric powder (P25 alone or dispersed inside the W740X suspension) and 50 wt% of submicrometric powder with the required amount of the polyacrylic deflocculant. The suspensions were prepared by adding first the PAA required to disperse both the nanosized titania (4 wt% with regard to titania) and the submicrometer sized one (0.5 wt%) to water or to the colloidal titania suspension, followed by the addition of the titania nanopowder and sonication for 1 min. In a second step the submicrometric powder was added and the mixture was maintained by 15 min. under mechanical agitation. Given PAA contents refer to the active matter

concentration. Figure 1 shows a scheme of the procedure followed to prepare the suspensions. Mixtures were labelled as 30M, 15P15M, and 10W5P15M, for submicronic titania Merck (M), mixture of P25 and M, and mixture of the three powders, respectively.

Rheological behaviour of all prepared suspensions was determined using a rheometer (RS50, Haake Thermo, Germany) operating at controlled shear rate (CR). Flow curves were obtained with a three-stage measuring program with a linear increase in the shear rate from 0 to 1000 s^{-1} in 300 s, a plateau at 1000 s^{-1} for 60 s, and a further decrease to zero shear rate in 300 s. The measurements were performed at 25 ºC using a double-cone and plate system.

Concentrated suspensions were slip cast in plaster moulds to obtain discs with 2 cm in diameter. The density of the cast specimens (green and presintered) was measured by the Archimedes' method using mercury and water, respectively.

Constant heating rate (CHR, heating and cooling rates 5 ºC/min) experiments up to 1600 ºC were performed in a differential dilatometer with alumina rod (DI24, Adamel Lhomargy, France). From the results of the dilatometer and DTA-TG analyses the temperatures of interest were selected (800 and 1000 ºC) and new specimens were prepared by quenching from those temperatures using the same heating rates. The quenched specimens were characterised as pieces by X-ray diffraction using a XRD diffractometer (D8 Advance, Bruker AXS, Germany). The microstructures of fracture samples were characterized by field emission gun-scanning electron microscopy with energy dispersive X-ray microanalysis, FE-SEM-EDX (S-4700 type I, Hitachi Japan). Pore distribution was measured by Mercury Intrusion Porosimetry (MIP, Poremaster, Quantachrome Corp., USA).

Results and discussion

The colloidal stability of the different starting materials is plotted in figure 2, which shows the variation of zeta potential with pH before and after the addition of the better concentration of polyelectrolyte as it was established in previous studies concerning on the stability of either the submicrometer sized or the nanosized powders used herein. The isoelectric point of the P25 nanopowder changes from pH 7 to pH 4 after the addition of 4 wt% of deflocculant as reported before [26]. The equivalent commercial suspension (W740X) has the isoelectric point at pH 6, slightly lower than that of the dry powder, this being a clear indication of the presence of some organic adsorbed on the surface of the particles [27]. The zeta potential does not change with the addition of PAA, which supports previous statement that colloidal titania particles have full coverage and there are no free sites to be filled by the PAA molecules. The isoelectric point of the submicrometer sized powder occurs at pH 5. The presence of PAA shifts down the IEP by only one pH unit.

Concentrated suspensions were always prepared to a total solids loading of 30 vol.% and the dispersion was improved changing the homogenisation time by ultrasounds. Firstly, the rheological behaviour of submicron sized powder suspensions (30M) was optimised. Figure 3 shows the flow curves of these suspensions prepared with different US times. The best results are obtained after 2–3 min sonication, where suspensions have very low viscosity (c.a. 12 mPa·s) and slightly shear thinning behaviour without thixotropy.

Secondly, bimodal 15P15M suspensions were prepared. Figure 4 shows the corresponding flow curves. The viscosities are significantly higher due to the presence of nanosized particles. Very low viscosities are obtained after sonication times of 5–7 min, the curves showing shear thinning behaviour and no thixotropy.

Finally, the 3-component10W5P15M suspensions were prepared maintaining a ratio of submicron to nanosized particles of 1:1 and a total solids content of 30 vol.%. The substitution of solid nanoparticles by the colloidal suspension reduces the viscosity of the bimodal suspension allowing better flowability for shaping. Figure 5 shows the corresponding flow curves. The lowest viscosity is reached after 6-7 min sonication.

Samples of all these mixtures were obtained at the optimum dispersing conditions by slip casting in plaster moulds. The density of the green specimens is shown in table 2. The densities of 30M cast specimens are also shown. These cast samples give a relative green density of 56%, whereas the 15P15M mixture leads to the highest densities, above 65% TD. This demonstrates that there is an effective packing of the smaller particles in the voids left by the larger ones, when nanoparticles were added. However, in the case of the 10W5P15M mixture, the green density is lower than in the case of the 15P15M mixture, although it is still higher than the green density of the submicrometer sized titania compacts. Considering that the viscosity of this mixture is lower, a higher density should be expected. This result could be related to a faster migration of the colloidal particles through the cake during filtration process. More work would be necessary to demonstrate this point, but it is outside the scope of this study.

To evaluate the sintering behaviour dilatometric experiments were performed using green slip cast bodies. The shrinkage curve of submicrometer sized titania (Merck), reported in a previous work [37] showed two significant slope changes that were highlighted in the derivative curve (Figure 6a). The first one, occurring at about 1060 ºC was identified as the transformation of anatase to rutile, which involves a sudden shrinkage of about 8.5 vol.% (calculated using the theoretical densities of anatase–TiO_2, 3.89 g/cm^3, and rutile-TiO_2, 4.25 g/cm^3). This transformation can occur between 400 and 1200 ºC depending on several parameters, such as grain size, impurities and

atmosphere [38,39]. The second slope change (~1220 ºC) corresponded to the maximum shrinkage rate and it was wider than the previous one indicating that it is a progressive process. Shrinkage was arrested at ~1400 ºC. When the nanopowders are added to the submicron sized titania, the behaviour is different, as observed in figure 6b. The first peak associated to phase transformation centred at 950 ºC has a shoulder that can be associated to necks formation among nanoparticles, and the second peak, corresponding to maximum shrinkage rate appears at 1170 ºC (figure 6a). That is, the temperature of the characteristic processes decreased due to the higher activity of the nanoparticles. The 10W5P15M mixture led to a similar behaviour but the characteristic temperatures of the minima were slightly higher, 970 ºC and 1190 ºC (figure 6c). In all cases there was a continuous progress of shrinkage, and densification slightly increased until a sintering temperature of 1500 ºC. This was expected because the presence of the submicrometer sized particles determines the densification temperature.

From these results new samples of the 10W5P15M mixture were prepared and quenched at 800 ºC and 1000 ºC in order to know the phases at these characteristic temperatures before and after phase transformation. The XRD patterns shown in figure 7 demonstrate that at 1000 ºC most of the anatase has transformed to rutile phase, while at 800 ºC the anatase remains as the major phase. The microstructure of the obtained specimens can be seen in the pictures of figure 8. An open microstructure is obtained at both temperatures, as expected from dilatometric results, but the grain size strongly increases in the specimens treated at 1000 ºC in agreement to the transformation to rutile phase. Therefore, all nanoparticles have grown and no differences are found when naonosize titania is added to submicron sized one.

Table 3 summarizes the data obtained by MIP for the quenched samples and its pore size distribution is shown in figure 9. It is observed that the pore diameter is a function

of the temperature in addition to particle size. The material obtained by quenching at 800 ºC has higher porosity and finer pore size, and consequently it has a significantly higher total pore area. For the production of porous titania materials with photocatalytic properties, the presence of some anatase phase has been reported elsewhere to be essential. Then, the porous materials obtained in this work by slip casting and treated at 800 ºC are expected to be suitable candidates for the desired photocatalytic applications.

Conclusions

Concentrated bimodal suspensions of titania were prepared to a total solids content of 30 vol.% with a ratio of submicrometer to nanosized particles of 1:1. The viscosities of bimodal suspensions are higher than submicrometer sized suspension with the same solids loading. Very low viscosities are obtained after sonication times of 5–7 min, the curves showing shear thinning behaviour and no thixotropy. The partial substitution of nanoparticles by the colloidal suspension leads to a significant reduction of viscosity.

The shrinkage curve of submicrometer sized titania showed a first peak at 1060 ºC corresponding to the transformation of anatase to rutile and a second slope change at 1220 ºC that corresponds to the maximum shrinkage rate. When the nanopowders are added to the submicron sized titania, the first peak appears at 950 ºC and has a shoulder that can be associated to necks formation among nanoparticles, and the maximum shrinkage rate occurs at lower temperature, 1170-1190 ºC. XRD patterns of bimodal porous samples quenched at 800 ºC and 1000 ºC show that at 1000 ºC most of the anatase has transformed to rutile phase, but at 800 ºC the anatase remains as the major phase and has higher surface area and porosity, as desired for photocatalytic applications.

Acknowledgements

This work has been supported by MINECO (Spain, contracts MAT2012-31090, MAT2009-14144-C03-01, and MAT2012-38364-C03-01).

References

[1] A. Fujishima, X. Zhan, Titanium dioxide photocatalysis: present situation and future approaches, C. R. Chimie 9 (2006) 750–760.

[2] C. Wu, Y. Yue, X. Deng, W. Hua, Z. Gao, Investigation on the synergetic effect between anatase and rutile nanoparticles in gas-phase photocatalytic oxidation, Catal. Today 93-95 (2004) 863–69.

[3] S. Lei, W. Duran, Highly active mixed phase photocatalysts fabricated at low temperature and the correlation between phase composition and photocatalytic activity, J. Environ. Sci. 20 (2008) 1263–1269.

[4] N.N. Binitha, Z. Yaakob, M.R. Reshmi, S.Sugunan, V.K. Ambili, A.A. Zetty, Preparation and characterization of nano silver-doped mesoporous titania photocatalysts for dye degradation, Catal. Today 1475 (2009) 576–580.

[5] M. Saif, M.S.A.Abdel–Mottaleb, Titanium dioxide nanomaterial doped with trivalent lanthanide ions of Tb, Eu and Sm: Preparation, characterization and potential applications, Inorg. Chim. Acta, 360 (2007) 2863–2874.

[6] V. Stengl, S. Bakardjieva, N. Murafa, Preparation and photocatalytic activity of rare earth doped TiO_2 nanoparticles, Mater. Chem. Phys., 114 (2009) 217–226.

[7] J. Yu, J. Zhang, A simple template-free approach to TiO_2 hollow spheres with enhanced photocatalytic activity, Dalton Trans, 39 (2010) 5860–5867.

[8] M. Borlaf, H.M. Wu, M.T. Colomer, R. Moreno, W.J. Tseng, Synthesis and characterization of anatase-structured titania hollow spheres doped with erbium (III), J. Am. Ceram. Soc. 95 (2012) 3005–3011.

[9] L.L. Ren, Y.P. Zeng, D.L. Jiang , Preparation of porous TiO_2 sheets by aqueous tape casting and their photocatalytic activation, Int. J. Appl. Ceram. Technol.5 (2008) 505–512.

[10] T. Chartier, D. Merle, J.L. Besson, Preparation of porous TiO_2 sheets by aqueous. Laminar ceramic composites, J. Eur. Ceram. Soc. 15 (1995) 101–107.

[11] E. Lugscheider, K. Bobzin, A. Etzkorn, G. Syrakas, C.W. Siry, Graded EB-PVD-thermal barrier coatings produced by powder evaporation, Adv. Eng. Mater. 4 (2002) 919–922.

[12] T.M. Wang, S.K. Zheng, W.C. Hao, C. Wang, Studies on photocatalytic activity and transmittance spectra of TiO_2 thin films prepared by r.f. magnetron sputtering method, Surf. Coat. Technol. 155 (2002) 141–145.

[13] R.S Lima, B.R. Marple, Thermal spray coatings engineered from nanostructured ceramic agglomerated powders for structural, thermal barrier and biomedical applications: A review, J. Thermal Spray. Technol. 16 (2007) 40–63.

[14] J. Morgiel, E. Sánchez, J. Grzonka, E. Bannier, M. Vicent, L. Major, The microstructure of WC-12%Co plasma sprayed coatings obtained from micro- and nano-powders, Inzynieria Materialowa 28 (2007) 1–6.

[15] E. Sánchez, V. Cantavella, E.Bannier, M.D. Salvador, E. Klyastina, J. Morgiel, J. Grzonka, A.R.Boccaccini, Deposition of Al_2O_3-TiO_2 nanostructured powders by atmospheric plasma spraying, J. Therm. Spray Technol. 17 (2008) 329–337.

[16] N. Berger-Keller, G. Bertrand, C. Filiare, C. Meunier, C.Coddet, Microstructure of plasma-sprayed titania coatings deposited from spray-dried powder, Surf. Coat. Technol. 168 (2003) 281–290.

[17] X. Chen, H. Cheng, J.Ma, A study on the stability and rheological behavior of concentrated TiO_2 dispersions, Powder Technol. 99 (1998) 171–176.

[18] O. Lyckfeldt, D. Kack, K.Rundgren, Pressing and sintering developments of Freeze Granulated Si_3N_4 materials, Ceram. Eng. Sci. Proc. 24 (2003) 331–336.

[19] N. Uchida, T. Hiranami, S. Takada, K. Uematsu, Spray-freeze-dried granules for ceramics fabrication, Am. Ceram. Soc. Bull. 81 (2002) 57–60.

[20] Y. De Hazan, J. Heinecke, A. Weber, T.Graule, High solids loading ceramic colloidal dispersions in UV curable media via comb-polyelectrolyte surfactants, J. Colloid Interface Sci. 337 (2009) 66–74.

[21] M. Vicent, E. Sánchez, T. Molina, M.I. Nieto, R. Moreno, Comparison of freeze drying and spray drying to obtain porous nanostructured granules from nanosized suspensions, J. Eur. Ceram. Soc. 32 (2012) 1019–1028.

[22] B.P.C. Raghupathy, J.G.P. Binner, Spray Granulation of nanometric zirconia particles,. J. Am. Ceram. Soc. 94 (2011) 42–48.

[23] I. Santacruz, K. Annapoorani, J.G.P. Binner, Preparation of high solids content nano zirconia suspensions,. J. Am. Ceram. Soc. 91 (2008) 398–405.

[24] S. Fazio, J. Guzmán, M.T. Colomer, A. Salomoni, R. Moreno, Colloidal stability of nanosized titania aqueous suspensions, J. Eur. Ceram. Soc. 28 (2008) 2171–2176.

[25] B. Faure, J.S. Lindeløv, M. Wahlberg, N. Adkins, P. Jackson, L. Bergström, Spray drying of TiO_2 nanoparticles into redispersible granules, Powder Technol. 203 (2010) 384–388.

[26] M. Vicent, E. Sánchez, I. Santacruz, R. Moreno, Dispersion of TiO_2 nanopowders to obtain homogeneous nanostructured granules by spray-drying, J. Eur. Ceram. Soc. 31 (2011) 1413–1419.

[27] M. Vicent, E. Sánchez, I. Santacruz, A. Moreno, R. Moreno, Preparation of high solids content nanotitania suspensions to obtain nanostructured spray-dried powders for atmospheric plasma spraying, J. Eur. Ceram. Soc. 32 (2012) 185–194.

[28] C.P. Cameron, R. Raj, Better sintering through green state deformation processing, J. Am. Ceram. Soc. 73 (1990) 2032–2037.

[29] J.C. Chang, F.F. Lange, D.S. Pearson, J.P. Pollinger, Pressure sensitivity for particle packing of aqueous alumina slurries vs. interparticle potential, J. Am. Ceram. Soc. 77 (1994) 1357–1360.

[30] U. Aschauer, .Burgos-Montes, R. Moreno, P. Bowen, Hamaker 2: a toolkit for the calculation of particle interactions and suspension stability and its application to mullite synthesis by colloidal methods, J. Dispersion Sci. Techn. 32 (2011) 470–479.

[31] N. Garmendia, I. Santacruz, R. Moreno, I. Obieta, Slip casting of nanozirconia-MWCNT composites using a heterocoagulation process, J. Eur. Ceram. Soc. 29 (2009) 1939–1945.

[32] J.H. Pan, H.Q. Dou, Z.G. Xiong; C. Xu, J. Ma, X.S. Zhao, Porous photocatalysts for advanced water purifications, J. Mater. Chem. 20 (2010) 4512-4528.

[33] A. Natoli, A. Cabeza, A.G. De la Torre, M.A.G. Aranda, I. Santacruz, Colloidal processing of macroporous TiO_2 Materials for photocatalytic water treatment, J. Am. Ceram. Soc. 95 (2012) 502-508.

[34] A.R.S. Studard, U.T. Gonzenbach, E. Tervoort, L.J. Gauckler, Processing routes to macroporous ceramics: a review, J. Am. Ceram. Soc, 89 (2006) 1771-1789.

[35] M. Scheffler, P. Colombo (eds.), Cellular ceramics. Structure, manufacturing, properties and applications, Wiley-VCH, Germany, 2005.

[36] T. Ohno, K. Sarukawa, K. Tokieda, M. Matsumura, Morphology of a TiO_2 photocatalyst (Degussa P-25) consisting of anatase and rutile crystalline phases, J. Catal. 203 (2001) 82-86.

[37] E. López-López, M.L. Sanjuán, R. Moreno, C. Baudín, Phase evolution in reaction sintered zirconium titanate based materials, J. Eur. Ceram. Soc. 30 (2010) 981-991.

[38] R.D. Shannon, J.A. Pask, Kinetics of the anatase–rutile transformation, J. Am. Ceram. Soc. 48 (1965) 391-398.

[39] P.I. Gouma, M.J.Mills, Anatase-to-rutile transformation in titania powders, J. Am. Ceram. Soc 84 (2001) 619–22.

Table 1. Characteristics of the starting materials

PROPERTY	MERCK	P25	W740X*
Major phase	A	A (R)	A (R)
Ss (m^2/g)	9	39	32
$D_{v,50}$ (nm)	350	21	20
Purity (%)	99.5	99.5	99.5
Density (g/cm^3)	3.87	3.76	-
Weight loss (%)	0.5	2.5	4.5

* Properties of the nanopowder dried from the colloidal suspension

Table 2. Green densities of the slip cast bodies produced with the different mixtures.

Sample	Absolute density (g/cm^3)	Relative density (% TD)
30M	2.20	56.0
15P15M	2.55	65.5
10W5P15M	2.26	58.1

Table 3. Density and porosity data of samples produced with the mixture of the three powders (10W5P15M) quenched at 800 and 1000 ºC.

T (ºC)	ρ (g/cm^3)	ρ_r (% TD)	V_{pore} (cm^3/g)	d_{pore} (nm)	Porosity (%)	A_{pore} (m^2/g)
1000	2.97	70.5	0.11	85	31.5	5.2
800	2.31	59.5	0.16	23	37.0	27.4

Captions to figures

Figure 1. Scheme of the procedure followed to prepare the suspensions of the mixtures.

Figure 2. Variation of zeta potential with pH of the starting powders as received and After the addition of the optimum deflocculant content.

Figure 3. Flow curves of 30M suspensions prepared with different US times.

Figure 4. Flow curves of bimodal 15P15M suspensions prepared with different US times.

Figure 5. Flow curves of 3-component10W5P15M suspensions prepared with different US times.

Figure 6. Dilatometry curves and derivatives of 30M (a), bimodal 15P15M (b), and 3-component10W5P15M (c) suspensions.

Figure 7. XRD patterns of 10W5P15M samples quenched at 800 ºC and 1000 ºC.

Figure 8. FE-SEM pictures of 10W5P15M samples quenched at 800 ºC (a,b) and 1000 ºC (c,d).

Figure 9. Pore diameter distribution of 10W5P15M samples quenched at 800 ºC and 1000 ºC.

Figure 1. Scheme of the procedure followed to prepare the suspensions of the mixtures.

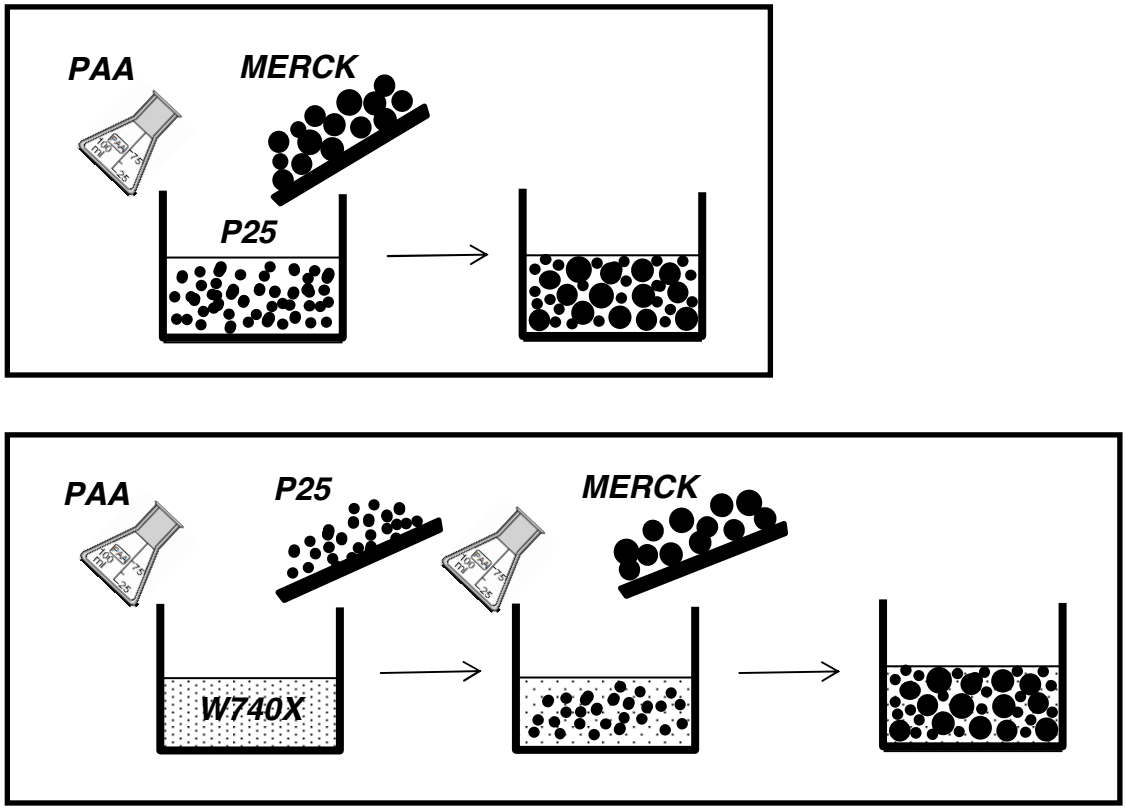

Fig. 1

Figure 2. Variation of zeta potential with pH of the starting powders as received and After the addition of the optimum deflocculant content.

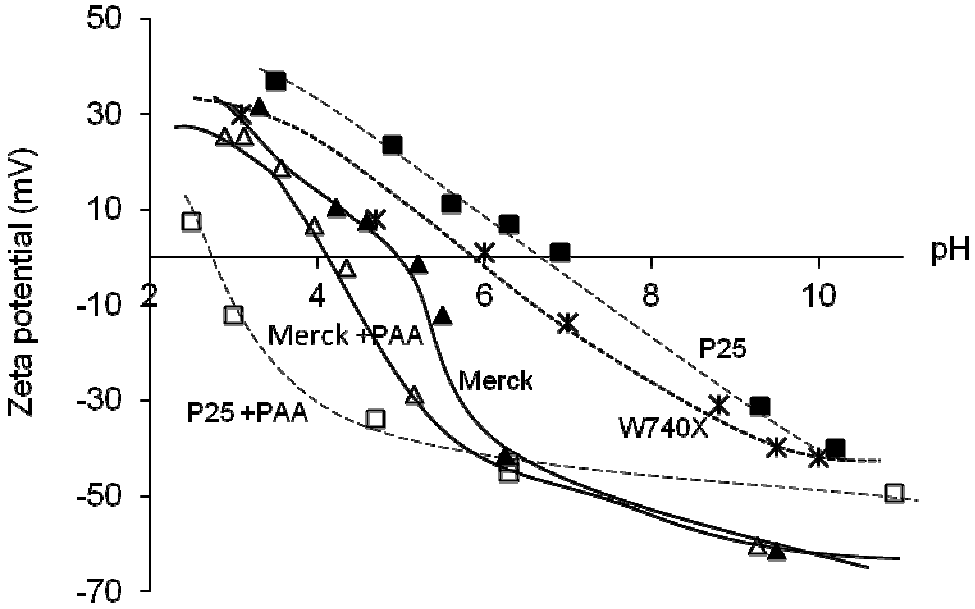

Fig. 2

Figure 3. Flow curves of 30M suspensions prepared with different US times.

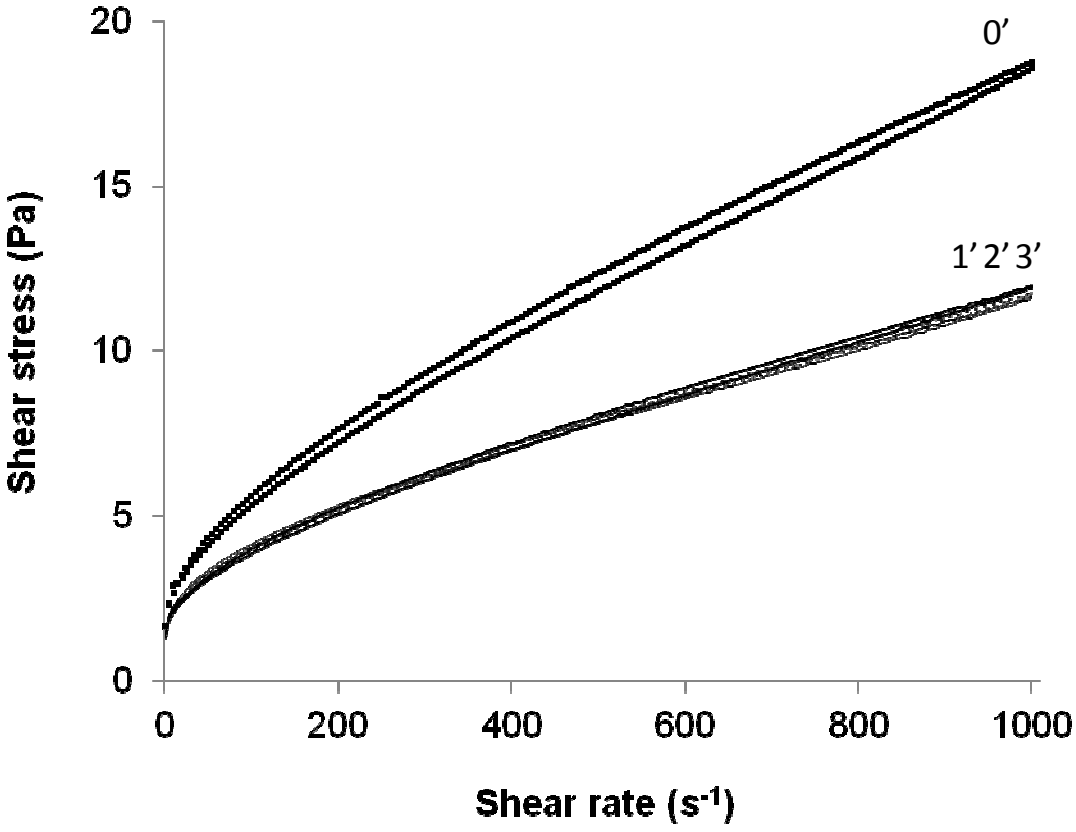

Fig. 3

Figure 4. Flow curves of bimodal 15P15M suspensions prepared with different US times.

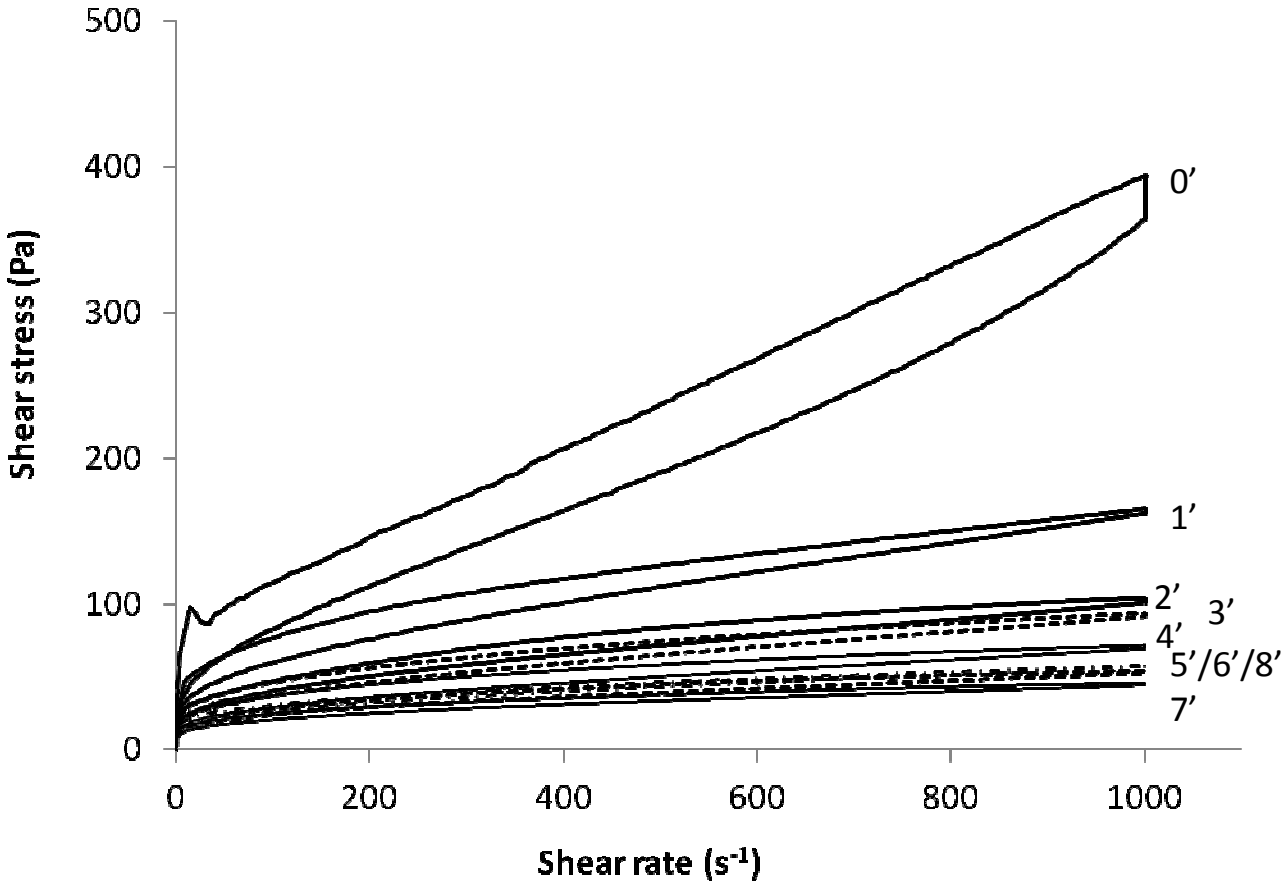

Fig. 4

Figure 5. Flow curves of 3-component10W5P15M suspensions prepared with different US times.

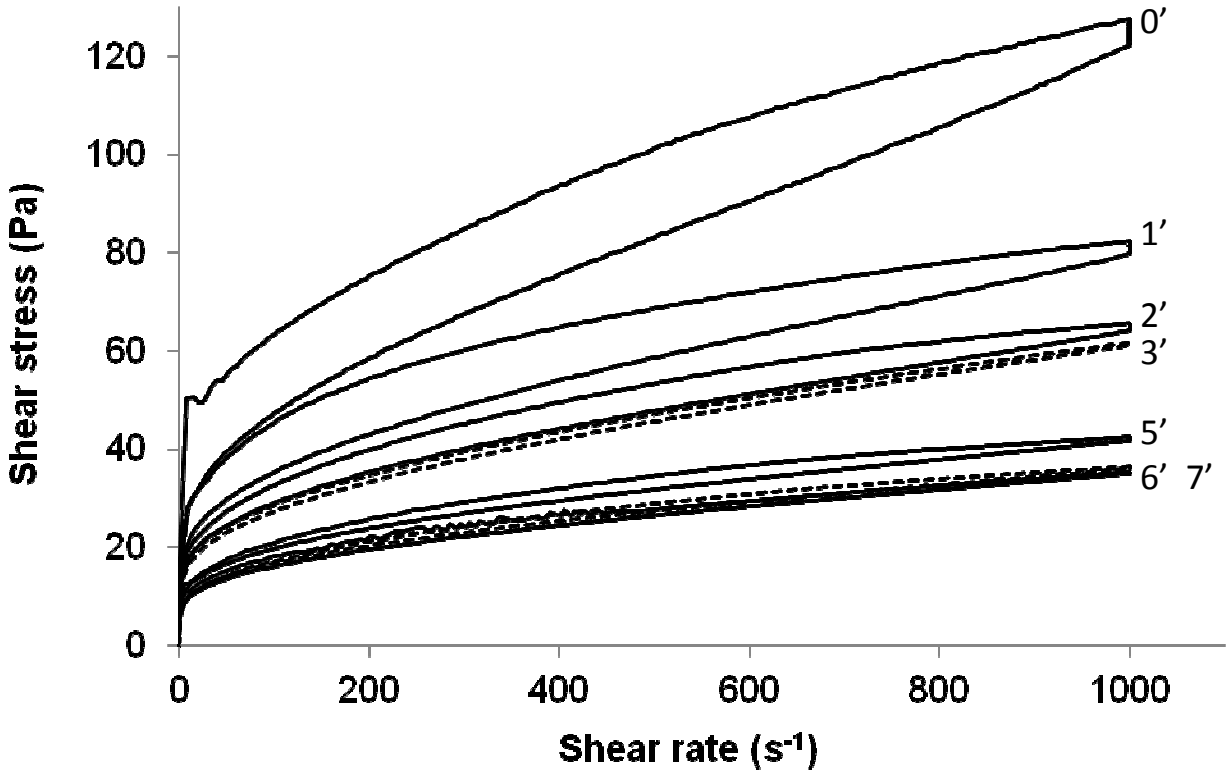

Fig. 5

Figure 6. Dilatometry curves and derivatives of 30M (a), bimodal 15P15M (b), and 3-component10W5P15M (c) suspensions.

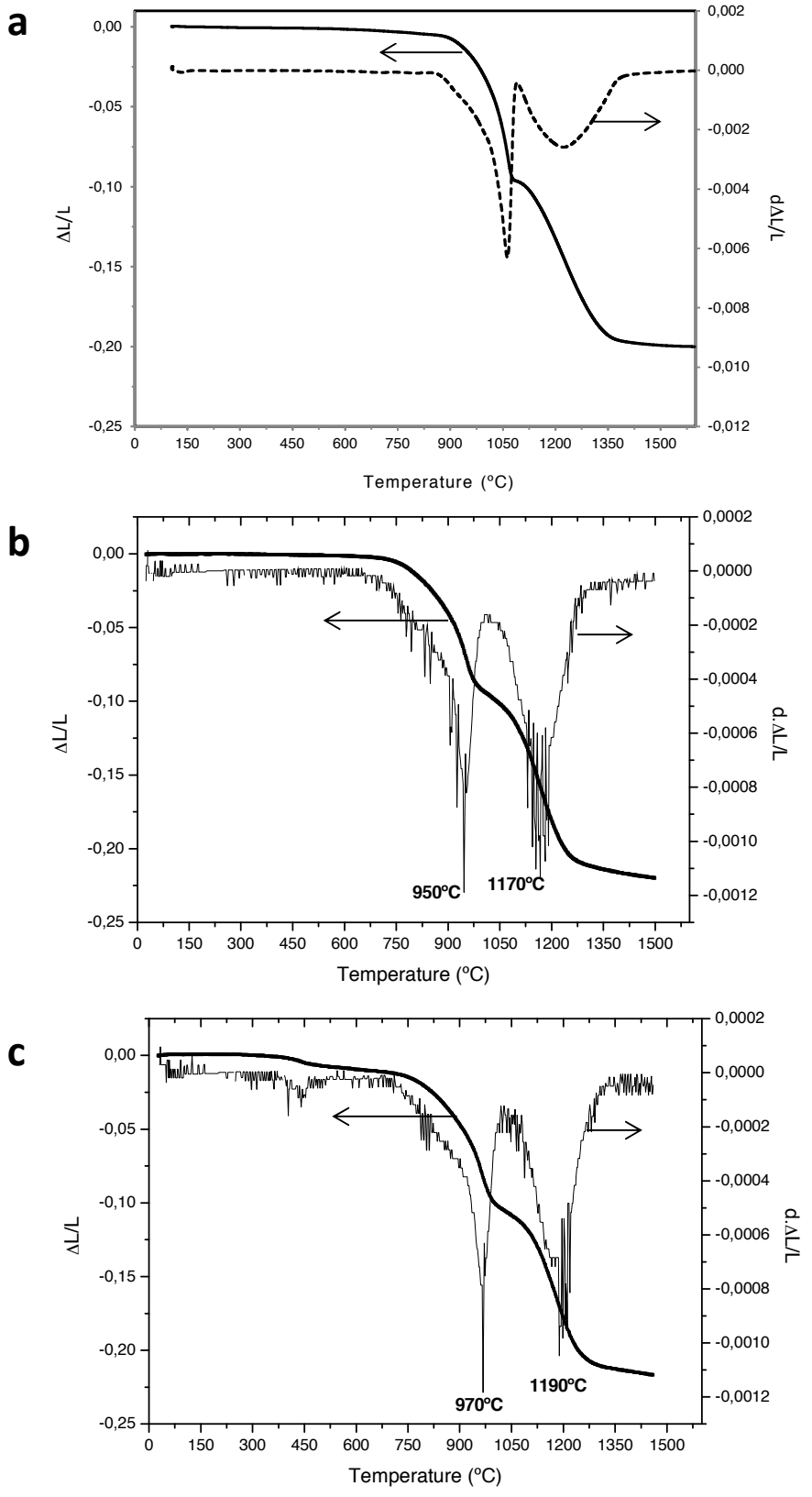

Figure 7. XRD patterns of 10W5P15M samples quenched at 800 ºC and 1000 ºC.

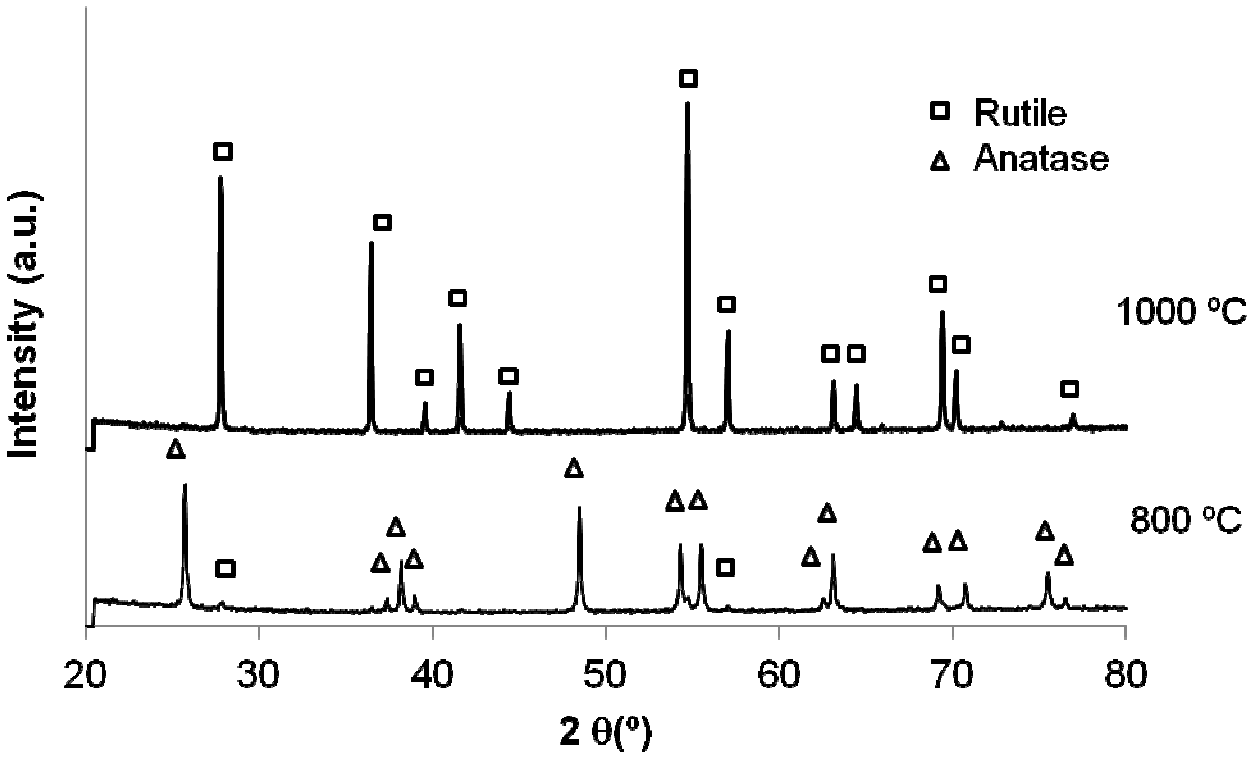

Fig. 7

Figure 8. FE-SEM pictures of 10W5P15M samples quenched at 800 ºC (a,b) and 1000 ºC (c,d).

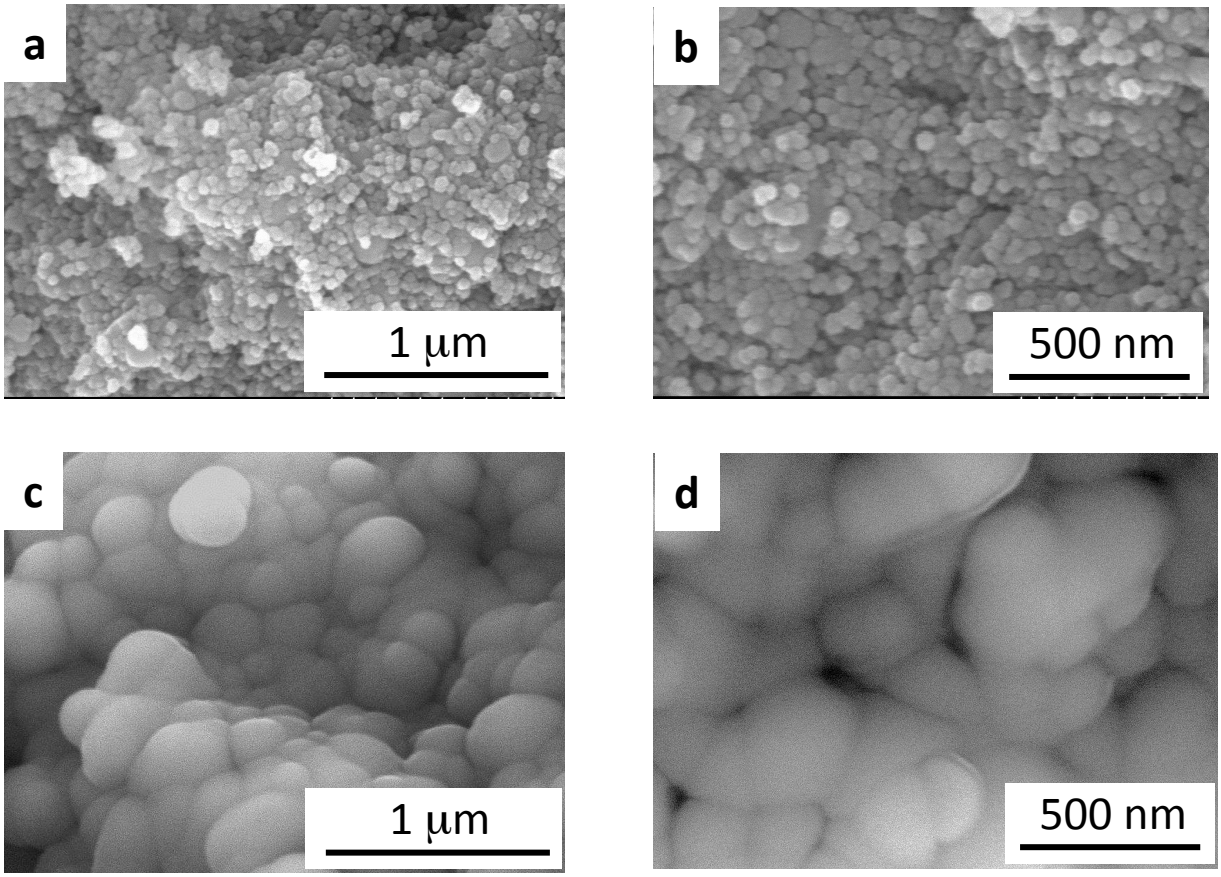

Fig. 8

Figure 9. Pore diameter distribution of 10W5P15M samples quenched at 800 ºC and 1000 ºC.

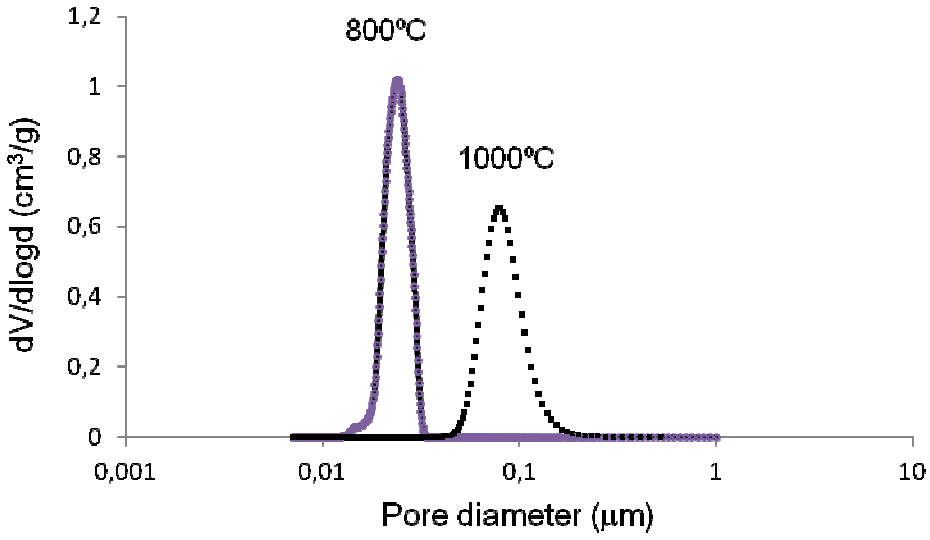

Fig. 9